KOREAN JOURNAL OF PACKAGING SCIENCE & TECHNOLOGY
Vol. 31, No. 3 195~201 (2025)
https://doi.org/10.20909/kopast.2025.31.3.195

PVA /Tea Leaf–Derived Carbon Quantum Dots Nanocomposites for Enhanced Barrier and Antimicrobial Food Packaging Films

Mohammadreza Jozaghkar, Jamilur R. Ansari, and Jongchul Seo*

Department of Packaging & Logistics, Yonsei University, 1 Yonseidae-gil, Wonju, Kangwon-do, 26493, South Korea

Abstract This study explores the multifunctional enhancement of polyvinyl alcohol (PVA) films through the incorporation of tea leaf–derived carbon quantum dots (CQDs) at loadings of 0.5, 1.0, 2.0, and 3.0 wt.%, focusing on structural, optical, mechanical, antimicrobial, and barrier properties. FTIR spectroscopy revealed strengthened hydrogen bonding and compatibility between PVA and CQDs, with broadened O-H stretching peaks indicating interactions with CQDs surface groups. XRD analysis showed preserved semi-crystalline PVA structure with increased crystallinity at higher CQDs loadings, suggesting uniform dispersion without phase separation. Photoluminescence spectra demonstrated strong blue emission from CQDs at 450 nm upon 360 nm excitation, attributed to quantum confinement and functional groups. Tensile testing indicated significant improvements in stress at break (from 25.01 MPa for pure PVA to 83.28 MPa at 3.0 wt.% CQDs) and Young's modulus (from 26.09 MPa to 115.84 MPa), highlighting reinforcement effects. Oxygen transmission rate decreased markedly from 6.32 cc/m²·day for pure PVA to 0.11 cc/m²·day at 3.0 wt.% CQDs. UV shielding was enhanced by the incorporation of CQDs, achieving complete UV-B blocking at 2.0 and 3.0 wt.% loadings and over 75% UV-A blocking at 3.0 wt.%, while maintaining visible transparency. Antibacterial disk diffusion assays exhibited concentration-dependent inhibition zones, maximizing at 3.0 wt.% CQDs, likely due to reactive oxygen species generation and electrostatic interactions.

Keywords Tea leaves, carbon quantum dots, polyvinyl alcohol, antimicrobial packaging, oxygen barrier, UV shielding

Introduction

Conventional petroleum-derived packaging materials provide effective protection for food products but generate significant environmental concerns due to their non-biodegradability[1,2]. The resulting plastic waste crisis has intensified research into sustainable and biodegradable alternatives that can offer equivalent or superior protective properties. Polyvinyl alcohol (PVA) is a promising candidate owing to its film-forming ability, mechanical strength, and oxygen barrier performance. However, its high hydrophilicity and limited antimicrobial properties restrict its broader application in food packaging[3,4].

Nanomaterial incorporation into polymer matrices has emerged as an effective strategy to overcome these limitations. Among them, carbon quantum dots (CQDs) have attracted attention due to their tunable surface chemistry, excellent dispersibility, photoluminescence, and antimicrobial activity. Recent studies have shown that CQDs can enhance polymer crystallinity, mechanical reinforcement, UV shielding, and barrier properties, making them suitable for active packaging applications. Importantly, CQDs derived from renewable biomass precursors provide additional environmental benefits compared with conventional synthesis routes[5-7].

Tea leaves, a biomass waste generated in large quantities from forestry and landscaping, are an abundant and underutilized precursor for green nanomaterials. Their high carbon content and natural polyphenolics make them ideal for the sustainable synthesis of CQDs via hydrothermal carbonization. Biomass-derived CQDs not only reduce waste but also offer inherent antimicrobial and antioxidant activities, which can be harnessed in food preservation[8,9].

Although several studies have explored the incorporation of nanomaterials such as graphene oxide, cellulose nanocrystals, and CQDs from various biomass sources (e.g., fruit peels, agricultural residues, and lignin) into polymer matrices for food packaging, limitations remain. Many biomass-derived CQDs reported to date provide moderate improvements in UV shielding and barrier performance but show variable antimicrobial efficiency. Moreover, few studies have systematically examined the integration of biomass CQDs with PVA to balance barrier, antimicrobial, and mechanical properties. Tea leaves are an abundant, renewable, and underexploited precursor rich

*Corresponding Author: Jongchul Seo
1 Yonseidae-gil, Wonju, Kangwondo 26493, South Korea
Tel: +82-33-760-2774
E-mail: jcseo@yonsei.ac.kr

in aromatic compounds, which may yield CQDs with enhanced antimicrobial and antioxidant functionalities. However, their application in the development of biodegradable nanocomposite films has not been extensively investigated. This gap underscores the need to explore tea leaf–derived CQDs as sustainable nanofillers to advance the multifunctionality of PVA-based food packaging[10-12].

In this study, waste green tea leaves were chosen as a carbon source due to their rich carbon matrix and nitrogen-containing polyphenols, enabling the synthesis of self-doped CQDs without additional reagents. We hypothesize that CQDs will enhance the barrier properties of PVA by reducing oxygen transmission and increasing hydrophobicity, while simultaneously imparting antimicrobial effects against foodborne pathogens. To test this, PVA/CQDs nanocomposite films were fabricated at varying loadings and systematically characterized for their structural, optical, barrier, mechanical, and antimicrobial properties. The outcomes of this work highlight the potential of biomass-derived quantum dots as eco-friendly nanofillers for advanced food packaging applications.

Experimental

1. Materials and Methods

1.1. Synthesis of Tea Leaf–Derived CQDs

Dried and powdered waste black tea leaves (2 g) were dispersed in 40 mL of distilled water and hydrothermally treated at 200°C for 6 h in a Teflon-lined autoclave. After cooling, the solution was centrifuged (10,000 rpm, 10 min) and filtered (0.22 μm) to remove large particulates. The filtrate containing CQDs was dialyzed (1 kDa cutoff) for 24 h and stored at 4°C.

1.2. Preparation of PVA/CQDs Films

A 10 wt.% aqueous PVA solution was prepared by dissolving PVA at 90°C with constant stirring for 1 h. CQDs were then introduced into the PVA solution at loadings of 0.5, 1.0, 2.0, and 3.0 wt.% relative to PVA weight, followed by additional stirring for 2 h to ensure homogeneity. The mixed solutions were cast into Petri dishes and dried at 40°C for 48 h. The resulting films were peeled and conditioned at 25°C and 50% RH before testing.

The final film thickness was in the range of 95-100 μm, measured at five random points using a digital thickness gauge. The CQD concentration range was selected to study concentration-dependent effects on film performance while avoiding CQD aggregation at higher loadings.

1.3. Characterization

Transmission electron microscopy (TEM) images of CQDs were obtained using a JEM-2100F JEOL microscope by placing a sample drop on a copper grid and evaporating it at room temperature. Fluorescence images of PVA and PVA/CQDs nanocomposite films were captured under UV light. Attenuated total reflection Fourier-transform infrared (FTIR) spectroscopy (65 FTIR, PerkinElmer) analyzed the chemical structure of pure PVA and PVA/CQDs nanocomposite films in transmission mode (4,000-400 cm^{-1}, 64 scans, air as reference). X-ray diffraction (XRD) using a Smart Lab diffractometer (Ultima IV, Rigaku, $\lambda = 0.1539$ nm) characterized the nanocomposite films, with intensities normalized over $2\theta = 58^{o} – 60^{o}$. Mechanical properties were evaluated using a Universal Tensile Strength Machine (UTM, Qmesys Co., South Korea) to measure tensile strength and elasticity. Oxygen transmission rate (OTR) was assessed using OX-TRAN 702 (MOCON, USA), and film thicknesses were measured with a thickness tester. Antibacterial efficacy against *S. aureus* was tested via disk diffusion (JIS Z 2801:2010). *S. aureus* (ATCC 6538) was selected as the representative Gram-positive foodborne bacterium due to its prevalence in food contamination and human pathogens. The bacterial suspension was adjusted to 0.5 McFarland standard (≈1×10^{8} CFU/mL). Sterile film samples (25 mm diameter) were placed on inoculated tryptic soy agar plates and incubated at 37°C for 24 h. The inhibition zone diameter was measured using a digital caliper, and results were reported as mean ± SD from three independent tests.

Results and Discussion

1. Morphological Analysis of the synthesized CQDs

The microstructure and morphology of the synthesized CQDs were analyzed using transmission electron microscopy (TEM) and high-resolution transmission electron microscopy (HR-TEM). The monodispersity and spherical morphology of the synthesized CQDs are presented in Figure 1a. HR-TEM images clearly reveal lattice fringes of CQDs with an interplanar spacing of 0.21 nm, corresponding to the (001) crystal plane of carbon. The particle size distribution histogram of the synthesized CQDs (Figure 1b) indicates that the CQDs have diameters below 10 nm, with an average particle size of 3-4 nm[12,13].

2. PL analysis of the synthesized CQDs

The photoluminescence (PL) properties of the synthesized CQDs were investigated, as shown in Figure 2. The PL spectra consist of excitation (blue line) and emission (red line) spectra, measured in the 350-650 nm wavelength range. The excitation spectrum exhibits maximum intensity at approximately 360 nm, indicating the optimal excitation wavelength for CQDs. When excited at this wavelength, the emission spectrum peaks at 430 nm, demonstrating strong blue luminescence. The Stokes shift, calculated as the difference between excitation and emission maxima, highlights energy losses due to vibrational relaxation and solvent interactions within the CQDs structure.

Inset images display the visual appearance of the CQDs solution under visible light (left) and under UV (right). The

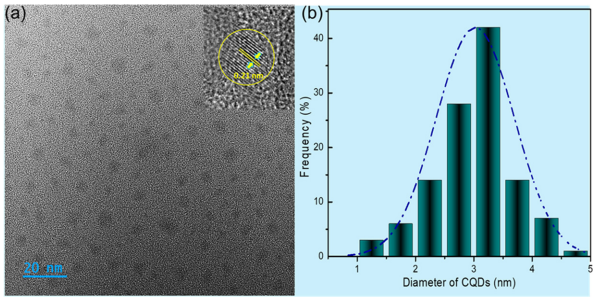

Fig. 1. (a) TEM of CQDs with 20 nm magnification (inset shows HR-TEM of CQDs with lattice structure of 0.21 nm) and (b) particle size distribution histogram

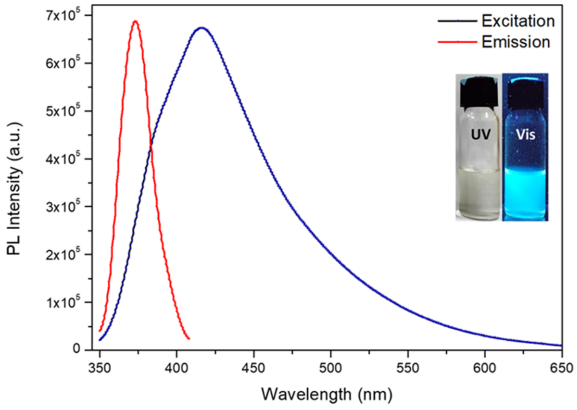

Fig. 2. PL spectra of the synthesized CQDs.

synthesized CQDs appear as a colorless solution under visible light, and bright blue luminescence under UV irradiation, corroborating the PL data. This blue luminescence is attributed to quantum confinement effects and the presence of surface functional groups (e.g., hydroxyl and carboxyl groups), which promote radiative recombination of excitons. The observed PL properties suggest the potential of CQDs for applications in food packaging, leveraging their tunable emission and high quantum yield[14-16].

3. Structural Analysis of PVA/CQDs nanocomposite films

Figure 3 presents the FTIR spectra of pure PVA and PVA/CQDs nanocomposites with varying CQDs loadings (0.5, 1.0, 2.0, 3.0 wt.%). The spectra were recorded in transmission mode over the 4,000-500 cm^{-1} wavenumber range. All samples exhibit characteristic PVA absorption bands, including a broad O-H stretching vibration at 3,300 cm^{-1} due to intermolecular hydrogen bonding, asymmetric and symmetric C-H stretching modes at 2,940 cm^{-1} and 2,850 cm^{-1}, a CH_2 bending vibration at ~1,430 cm^{-1}, and a C-O stretching vibration at 1,090 cm^{-1}.

The addition of CQDs induces subtle changes in these bands, with the O-H peak broadening and intensifying as

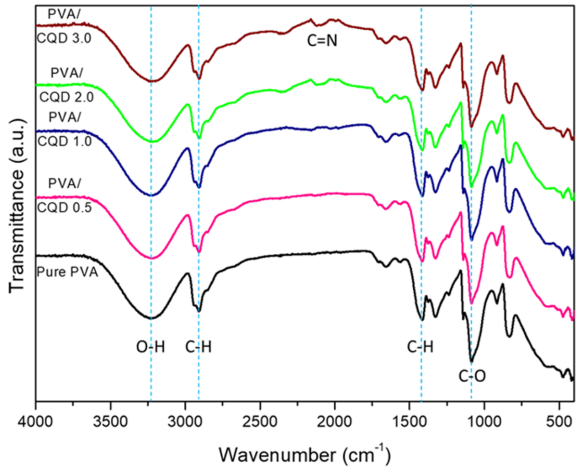

Fig. 3. FT-IR spectra of PVA/CQDs nanocomposite films.

CQDs concentration increases, suggesting enhanced hydrogen bonding interactions between PVA hydroxyl groups and CQDs functional groups (e.g., carboxyl or hydroxyl). Additionally, a slight intensity increase in the C=O and C-O bands is observed with higher CQDs content, reflecting contributions from oxygenated surface groups of CQDs. The overall spectral profiles remain similar across samples, confirming excellent compatibility and uniform dispersion of CQDs within the PVA matrix. Unlike pure PVA, the nanocomposite films exhibit a characteristic peak at around 2200 cm^{-1}, indicating successful nitrogen doping of CQDs[17-19].

4. UV Vis Transmittance analysis of PVA/CQDs nanocomposite films

The selective attenuation of UV-Vis by PVA/CQDs nanocomposite films arises from electronic transitions in the car-

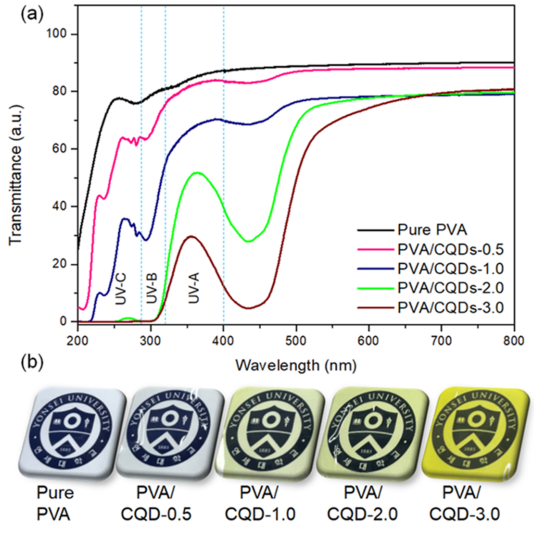

Fig. 4. (a) UV-spectra and (b) appearance of PVA/CQDs nanocomposite films.

bonaceous domains and surface functional groups introduced during hydrothermal synthesis. The complete UV-B blocking was achieved for nanocomposites containing 2.0 and 3.0 wt.% of CQDs. Sample PVA/CQDs-3.0 also showed more than 75 % UV-A blocking, demonstrating the ability of biomass-derived CQDs to deliver targeted photoprotection without compromising product visibility. Thickness-normalized absorption coefficients indicate an increased effective absorption per unit thickness with higher CQDs loading, supporting the role of CQDs as efficient UV-absorbing nanofillers. This improvement is primarily attributed to the strong UV absorption properties of the synthesized CQDs. CQDs possess abundant π-conjugated domains and oxygen-containing functional groups such as carbonyl, hydroxyl, and carboxyl moieties. These structures facilitate π–π* and n–π* electronic transitions, enabling efficient absorption of UV photons. When CQDs are uniformly dispersed within the PVA matrix, they act as nano-sized UV filters, absorbing the harmful UV radiation before it can penetrate the film.

Moreover, the nanoscale dimensions of CQDs (<10 nm) provide an additional scattering effect, particularly for shorter wavelengths in the UV region[20]. This dual mechanism of UV photon absorption and scattering contributes to the overall enhancement of UV-shielding efficiency. As a result, the PVA/CQDs films block a substantial portion of UV light while maintaining relatively high transparency in the visible region, which is crucial for applications like food packaging, where visibility of the packaged product is essential.

5. XRD analysis of PVA/CQDs nanocomposite films

Figure 5 presents the X-ray diffraction (XRD) patterns of pure PVA and PVA/CQDs nanocomposite films with varying CQDs loadings. The diffraction patterns were recorded over a 2θ range of 10°-60°, enabling the characterization of the samples' structural properties. Pure PVA exhibits a broad diffraction peak centered at 19.5°, indicative of its semi-crystalline nature with a predominantly amorphous structure and random polymer chain orientation.

The addition of CQDs induces subtle changes in the diffraction profile. The primary peak at 19.5° persists across all CQDs-loaded samples, suggesting that the crystalline regions of PVA are largely preserved. However, as CQDs content increases, an increase in peak intensity is observed, particularly pronounced in the PVA/CQDs-3.0 sample. This phenomenon may reflect changes in crystallinity due to the nucleation effects of CQDs. No distinct new peaks corresponding to CQDs were detected, indicating excellent compatibility and uniform dispersion of CQDs within the PVA matrix, with no formation of independent CQDs crystalline phases[21]. These findings suggest that CQDs incorporation maintains the structural integrity of the PVA matrix while increasing its crystallinity degree, potentially influencing mechanical properties for applications in food packaging.

6. UTM analysis of PVA/CQDs nanocomposite films

The tensile properties of pure PVA and PVA/CQDs nanocomposite films were evaluated through stress-strain testing, as shown in Figure 6 and summarized in Table 1. The stress-strain curves reveal distinct mechanical behaviors across the samples. Pure PVA exhibits a stress at break of 25.01 ± 1.4 MPa with a strain at break of 95.86 ± 5.1% and a Young's modulus of 26.09 ± 0.3 MPa, indicative of its characteristic ductility and moderate stiffness. Incorporation of CQDs enhances the mechanical strength progressively with increasing CQDs content. PVA/CQDs-0.5 shows a stress at break of 33.48 ± 2.1 MPa, strain at break of 90.22 ± 4.8%, and Young's modulus of 37.10 ± 0.4 MPa; PVA/CQDs-1.0 reaches 54.06 ± 2.5 MPa, 80.74 ± 4.2%, and 66.95 ± 0.6 MPa; PVA/CQDs-2.0 achieves 71.89 ± 3.2 MPa, 78.04 ± 4.1%, and 92.11 ± 0.7 MPa; and PVA/CQDs-3.0 attains the highest values of 83.28 ± 3.7 MPa, 71.89

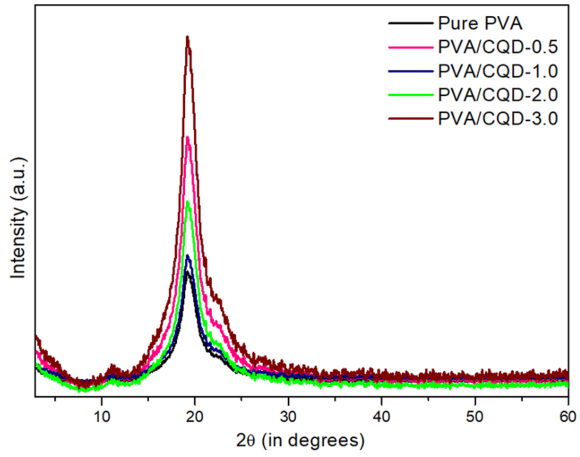

Fig. 5. XRD graph of PVA/CQDs nanocomposite films.

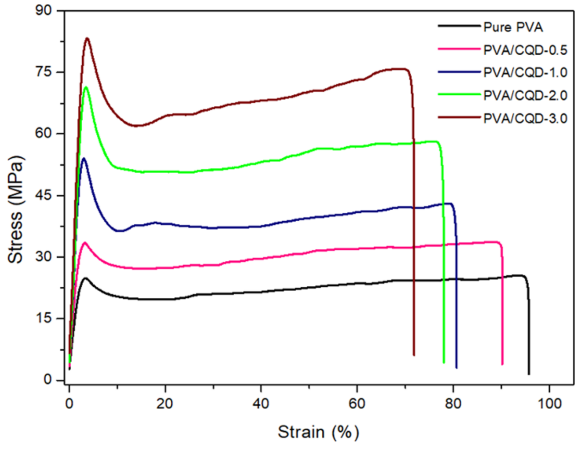

Fig. 6. Stress-strain curve of PVA/CQDs nanocomposite films.

Table 1. Mechanical and oxygen barrier characteristics of PVA/CQDs nanocomposite films

	Film Thickness (μm)	Stress (MPa)	Strain (%)	Young's Modulus (MPa)	OTR (cc/m^2.day)
Pure PVA	97.6 ± 1.4	25.01 ± 1.4	95.86 ± 5.1	26.09 ± 0.3	6.32 ± 0.8
PVA/CQDs (0.5)	98.2 ± 1.4	33.48 ± 2.1	90.22 ± 4.8	37.10 ± 0.4	0.58 ± 0.02
PVA/CQDs (1.0)	92.3 ± 1.3	54.06 ± 2.5	80.74 ± 4.2	66.95 ± 0.6	0.21 ± 0.01
PVA/CQDs (2.0)	98.9 ± 1.7	71.89 ± 3.2	78.04 ± 4.1	92.11 ± 0.7	0.16 ± 0.01
PVA/CQDs (3.0)	95.3 ± 1.2	83.28 ± 3.7	71.89 ± 3.9	115.84 ± 0.9	0.11 ± 0.01

± 3.9%, and 115.84 ± 0.9 MPa, respectively. The initial linear elastic region, followed by a yield point and subsequent plastic deformation, is evident in all samples, with pure PVA displaying the largest strain capacity before failure. The increase in stress at break and Young's modulus with higher CQDs loading suggests a reinforcing effect due to the uniform dispersion of CQDs within the PVA matrix, enhancing intermolecular interactions and load transfer. The observed reinforcement can be directly correlated with the structural evolution evidenced by FTIR and XRD analyses. The broadening of the O–H stretching band (Figure 3) suggests stronger hydrogen bonding between PVA hydroxyls and oxygenated CQD surfaces, enhancing load transfer efficiency under stress. Simultaneously, the intensified XRD peak at 19.5^o (Figure 5) indicates increased crystallinity, which contributes to stiffness and tensile strength. These combined effects explain the progressive mechanical improvement observed with higher CQD content. These findings highlight the potential of CQDs-reinforced PVA composites for applications requiring improved mechanical strength, such as food packaging, with the optimal CQDs loading depending on the desired balance between strength and flexibility[6,22].

7. Oxygen barrier performance of PVA/CQDs nanocomposite films

The oxygen transmission rate (OTR) of pure PVA and PVA/CQDs nanocomposite films was evaluated, as summarized in Table 1. The OTR values, expressed in cc/m^2·day, were measured for films with thicknesses ranging from 95.3 to 97.6 μm. Pure PVA exhibited an OTR of 6.32 ± 0.8 cc/m^2·day, reflecting its moderate oxygen permeability due to its semi-crystalline structure with inherent hydrophilic properties. The incorporation of CQDs significantly reduced the OTR, demonstrating a concentration-dependent barrier enhancement: PVA/CQDs-0.5 showed an OTR of 0.58 ± 0.02 cc/m^2·day, PVA/CQDs-1.0 reduced it to 0.21 ± 0.01 cc/m^2·day, PVA/CQDs-2.0 further decreased it to 0.16 ± 0.01 cc/m^2·day, and PVA/CQDs-3.0 achieved the lowest OTR of 0.11 ± 0.01 cc/m^2·day. This progressive reduction in OTR with increasing CQDs content is attributed to the uniform dispersion of CQDs within the PVA matrix, which likely creates a tortuous path for oxygen diffusion, enhancing the barrier properties. The slight variations in film thickness (e.g., 97.6 ± 1.4 μm for pure PVA vs. 95.3 ± 1.2 μm for PVA/CQDs-3.0) have a minimal impact on OTR, as the data are normalized per unit area and thickness effects are

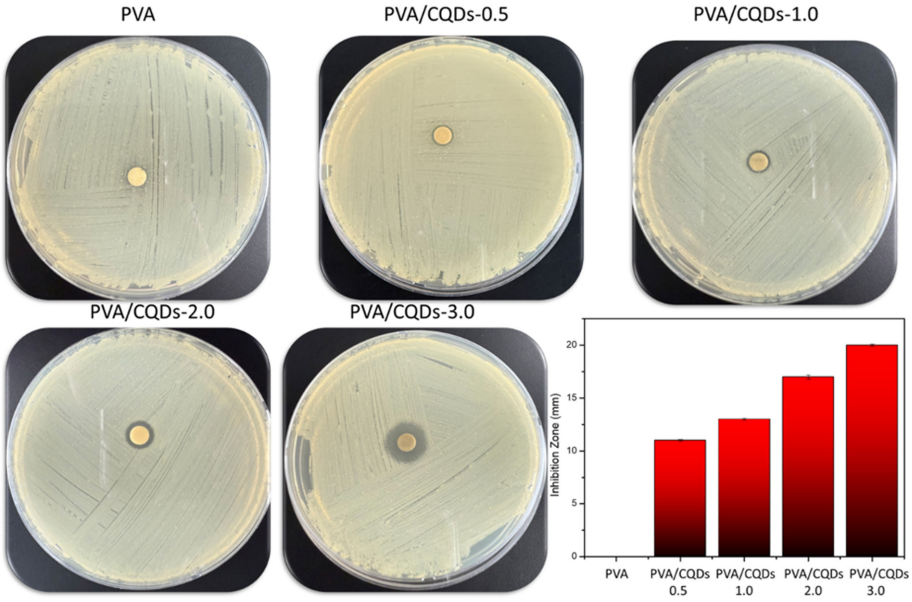

Fig. 7. Antibacterial activity of PVA/CQDs nanocomposite.

accounted for in standard testing protocols. These results suggest that CQDs-reinforced PVA films, particularly at higher loadings, are promising candidates for oxygen barrier applications, such as food packaging or protective coatings, where reduced oxygen permeability is critical to extend shelf life or prevent degradation[5,6,22].

8. Antibacterial Performance

The antibacterial efficacy of the pure PVA and PVA/CQDs nanocomposite films was evaluated using the standard disk diffusion assay, with results shown in Figure 7. Disks impregnated with the respective materials were placed at the center of agar plates inoculated with a bacterial lawn. After incubation, zones of inhibition were observed and compared. The pure PVA control exhibited no distinct zone of inhibition, indicating a lack of inherent antibacterial properties in the polymer matrix. In contrast, PVA/CQDs nanocomposites demonstrated a clear concentration-dependent enhancement in antibacterial activity. At 0.5 wt.% CQDs, the inhibition effect was minimal, but the zone of inhibition progressively widened at 1.0 and 2.0 wt.%, with the most pronounced antibacterial effect observed at 3.0 wt.% CQDs, where the inhibition zone extended significantly across the plate. The inhibition zones for PVA/CQDs films were 0, 11 ± 0.1, 13 ± 0.1, 17 ± 0.2, and 20 ± 0.1 mm for the films containing 0, 0.5, 1.0, 2.0, and 3.0 wt.% CQDs, respectively.

This trend underscores the critical role of CQDs in imparting antibacterial properties to the composites, primarily through mechanisms involving reactive oxygen species (ROS) generation, which induces oxidative stress and leads to cell membrane disruption. Additionally, the positively charged surface of CQDs promotes electrostatic interactions with negatively charged bacterial cell walls, enhancing adhesion and bactericidal effects. These findings highlight the potential of PVA/CQDs films as food packaging materials, offering tunable antibacterial performance to mitigate infection risks while maintaining biocompatibility[9].

Conclusion

This work demonstrates the successful synthesis of CQDs from tea leaves via a sustainable hydrothermal route and their effective incorporation into PVA to produce multifunctional nanocomposite films. The addition of CQDs significantly enhanced the films' physicochemical and functional properties, including mechanical strength, barrier performance, UV shielding, and antimicrobial activity. At optimal loading, tensile strength and Young's modulus improved, oxygen transmission decreased markedly from 6.32 to 0.11 cc/m^2 at 3.0 wt.% CQDs, and the films achieved complete UV-B blocking while maintaining high visible transparency. Antimicrobial assays confirmed strong inhibitory effects against *S. aureus* bacteria, verified the potential to extend shelf life through reduced microbial growth. These results highlight the potential of PVA/CQDs nanocomposites as biodegradable, sustainable, and active food packaging materials that address both environmental and food safety challenges. The use of an abundant biomass precursor such as tea leaves further underscores the green and circular nature of the approach.

Acknowledgements

The authors would like to express their appreciation to the Regional Innovation System & Education (RISE) program through the Gangwon RISE Center, funded by the Ministry of Education (MOE) and the Gangwon State (G.S.) [Grant No. 2025-RISE-10-001 & 2025-RISE-10-006].

References

1. Jozaghkar, M., Arabi, H., Heydari, F., Hasanpour, M. 2023. Effect of Microstructure on Rheological Behavior of Linear- and Branched-Polyethylene. Polymerization. 14(1), 55-59.
2. Jozaghkar, M., Jahani, Y., Arabi, H., Ziaee, F. 2017. Preparation and Assessment of Phase Morphology, Rheological Properties, and Thermal Behavior of Low-Density Polyethylene/Polyhexene-1 Blends: Polymer-Plastics Technology and Engineering: 57(8) 1344858.
3. Abdullah, Z. W., Dong, Y., Davies, I. J., Barbhuiya, S. 2017. PVA, PVA Blends, and Their Nanocomposites for Biodegradable Packaging Application. Polymer-Plastics Technology and Engineering 56, 1307-1344.
4. Jiang, S., Liu, S. Feng, W. 2011. PVA hydrogel properties for biomedical application. Journal of the Mechanical Behavior of Biomedical Materials 4, 1228-1233.
5. Ansari, J. R., Park, K., Sadeghi, K., Seo, J. 2025. Preparation of MoS2 modified with carbon quantum dots and its application to extremely high oxygen-barrier nanocomposite films for packaging. Food Packaging and Shelf Life 49, 101504.
6.vAnsari, J. R., Park, K., Seo, J. 2025. Improving the oxygen barrier properties of composite films using green tea extracted CQDs and PVA for active packaging applications. Food Packaging and Shelf Life 48, 101460.
7. Park, K., Ansari, J. R., Seo, J. 2025. Synthesis of white carbon quantum dots for the upcycling of highly durable olefin plastics. Materials Today Nano 31, 100670.
8. Namita, N., Ariba, K, Ansari, J. 2025. MoS2 quantum dots and their diverse sensing applications. emergent mater. 8, 2773-2803.
9. Han, S., Ansari, J. R., Park, K., Sadeghi, K. Seo, J. 2025. Carbon quantum dots synthesized from a lemon extract in ethyl acetate to enhance the performance of polylactic acid films for packaging applications. Journal of Industrial and Engineering Chemistry.
10. Zhao, Y., Yang, D., Yu, C., Yan, H. 2025. A review on pho-

tocatalytic CO2 reduction of g-C3N4 and g-C3N4-based photocatalysts modified by CQDs. Journal of Environmental Chemical Engineering 13, 115348.
11. Shariq, M. Alghamdi, G., Alotaibi, R. 2025. Design, synthesis, and structural engineering of carbon quantum dots and multifunctional N, P, B, S-doped CQDs for photocatalytic water purification. Journal of Water Process Engineering 77, 108450.
12. Huang, Y. Yu, Z, Huang, Y, Yan, W., Yang Z, 2026. Study on the performance and mechanism of NH2-MIL-101(Fe)/CQDs@UCN composite photocatalyst with self-Fenton effect. Materials Research Bulletin 194, 113716.
13. Jozaghkar, MR., Sepehrian Azar, A., Ziaee F., Mirtaleb F. 2022. Preparation, assessment, and swelling study of amphiphilic acrylic acid/chitosan-based semi-interpenetrating hydrogels. Turkish Journal of Chemistry 46(2), 499-505.
14. Latif, Z. 2024. Reinforcement using undoped carbon quantum dots (CQDs) with a partially carbonized structure doubles the toughness of PVA membranes. Nanoscale Adv. 6, 1750-1764.
15. Jozaghkar MR., Jahani, Y., Arabi, H., Ziaee F. 2019. Effect of polyethylene molecular architecture on the dynamic viscoelastic behavior of polyethylene/polyhexene-1 blends and its correlation with morphology." Polymer-Plastics Technology and Materials, 58(5) 560-572.
16. Mirtaleb, F., Jozaghkar, M. Ziaee, F., 2025. Controlled polymerization route to novel α-methyl styrene–olefin triblock copolymers with tailored architecture. Polyolefins Journal.
17. El-Shamy, A. G. Zayied, H. S. S. 2020. New polyvinyl alcohol/carbon quantum dots (PVA/CQDs) nanocomposite films: Structural, optical and catalysis properties. Synthetic Metals 259, 116218.
18. El-Shamy, A. G. 2019. Novel hybrid nanocomposite based on Poly(vinyl alcohol)/ carbon quantum dots/fullerene (PVA/CQDs/C60) for thermoelectric power applications. Composites Part B: Engineering 174, 106993.
19. El-Shamy, A. G. 2019. Novel conducting PVA/Carbon quantum dots (CQDs) nanocomposite for high anti-electromagnetic wave performance. Journal of Alloys and Compounds 810, 151940.
20. Gao, R. 2024. Phosphorus-doped carbon dots as an effective flame retardant for transparent PVA composite films with enhanced UV shielding property. Reactive and Functional Polymers 197, 105877.
21. Radhakrishnan, K. 2024. Sustainable synthesis of fluorescent polymer carbon dots@PVA for sensitive chlortetracycline detection. Luminescence 39, 4846.
22. Ansari, J. R., Park, K. Seo, J. 2025. Improving the oxygen barrier properties of composite films using green tea extracted CQDs and PVA for active packaging applications. Food Packaging and Shelf Life 48, 101460.

투고: 2025.09.29 / 심사완료: 2025.10.29 / 게재확정: 2025.11.06